AIAA JOURNAL
Vol. 36, No. 9, September 1998

Adaptive Grid Sequencing and Interpolation Schemes for Helicopter Rotor Wake Analyses

Ashish Bagai* and J. Gordon Leishman†
University of Maryland, College Park, Maryland 20742

Numerical acceleration schemes have been developed to improve the computational efficiency of free-vortex analyses of helicopter rotor wakes. Two general methodologies were formulated based on adaptive grid sequencing and velocity field interpolation schemes. Both approaches considerably reduce the number of induced velocity evaluations in free-vortex schemes but without significant loss in predictive accuracy of the wake geometry. The methods have been implemented and evaluated for a rotor wake analysis based on a pseudoimplicit predictor–corrector (PIPC) relaxation algorithm. The acceleration schemes were found to produce up to an order of magnitude decrease in execution times. Both methods are generic in formulation and application and may be adapted for use in other free-vortex methodologies. A third method that specifically exploits the pseudoimplicitness of the PIPC scheme has also been developed, resulting in further increases in computational efficiency.

Nomenclature

N_b = number of rotor blades
N_{CP} = total number of wake collocation points
N_E = number of Biot–Savart induced velocity evaluations
N_ζ = number of free collocation points per vortex filament
N_ψ = number of discrete azimuthal locations
n = number of rotor revolutions of free-vortex wake
$\boldsymbol{r}_{j,k}$ = collocation point position vector, m
$\boldsymbol{V}_{\text{ind}}$ = induced velocity vector, ms^{-1}
$\boldsymbol{V}_\infty$ = freestream velocity vector, ms^{-1}
$\Delta\zeta$ = vortex filament discretization resolution, deg
$\Delta\psi$ = azimuthal discretization resolution, deg
ζ_k = kth collocation point along vortex filament
μ = advance ratio
ψ_b = blade azimuthal location, deg
ψ_j = jth discretized azimuth location on rotor
Ω = rotor rotational frequency, rad s^{-1}

Introduction

THE ability to predict accurately the rotor aerodynamic environment is essential for the design of new rotorcraft with improved performance, increased maneuverability, reduced vibration levels, and lower noise. The next generation of military and civilian helicopters will be designed with significantly expanded flight envelopes and enhanced performance capabilities. Even short-term goals call for significant reductions in vibratory loads and rotor noise, as well as increased agility and aerodynamic efficiency. Therefore, a great deal of emphasis is being placed on improving the fidelity and overall capabilities of predictive tools for use in the aerodynamic design of advanced helicopters.

It has been well documented that the blade tip vortices are the most dominant structures in the wake of a helicopter rotor.[1] These vortical structures induce high local flow velocities and contribute significantly to the unsteadiness encountered by the rotor blades. Specific types of interactions between blades and tip vortices from preceding blades can produce airloads that lead to high localized pressure fluctuations over the blade surface, thereby resulting in the generation of impulsive noise. This blade vortex interaction (BVI) noise is particularly pronounced during maneuvering and descending flight conditions, where the blade tip vortices lie close to the rotor tip-path plane.[2] Moreover, the temporal variations in local blade angle of attack resulting from BVI can produce rotor vibrations that may limit the maneuvering capabilities and flight envelope of the aircraft.[3,4] For multirotor helicopters, such as tandems and coaxials, the BVI problem can be more acute because the vortices from one rotor may be directly ingested into the other rotor.[5]

Existing aerodynamic models available for use in the comprehensive engineering analysis of helicopter rotors range from blade-element/momentum theory to prescribed and free-vortex methods. More recently, the use of computational fluid dynamics (CFD) in the form of finite difference/finite volume solutions to the Navier–Stokes and Euler equations have been developed. In principle, CFD methods may be used to compute fundamental fluid properties,[6–13] on both the rotor blades and the wake. However, the degree of complexity associated with CFD schemes demand prohibitively high computational resources and, at present, can only be used as research tools. Moreover, issues such as grid construction, numerical stability, accuracy, and the artificial diffusion of vorticity further limit the practical use of many CFD analyses to helicopter rotor type problems.

Vortex methods, however, can be used much more routinely in rotor design. These approaches assume the existence of concentrated regions of vorticity in the flow, and the aerodynamic environment is determined by directly computing the induced contribution of discretized vortices to the net velocity field. In prescribed rotor wake models, the positions of the vortex filaments are specified using semiempirical equations.[14–17] Such models are, therefore, limited to the range of rotor operational conditions and blade geometric parameters for which measured wake data are available. A much more general approach is to allow the discretized vortex filaments to convect under the action of the local induced velocities to force-free locations, the so-called free-wake problem. The behavior of the vortex filaments is governed by the vorticity transport equation.[18] These free-wake methods provide a high degree of versatility and flexibility and have a minimal dependency on empiricism. However, the formulation of numerically robust, physically accurate, and computationally efficient free-wake schemes still remains inherently challenging to the helicopter rotor analyst.

Numerous free-wake solution methodologies have been developed over the past two decades, including relaxation approaches[19–27] and time-marching schemes.[28–33] The inherent nonlinearity of the problem means that many of the numerical methods used in these schemes do not converge or otherwise provide a unique wake solution and so cannot be used reliably. However, the main

Received April 4, 1997; presented as Paper 97-2327 at the AIAA 15th Applied Aerodynamics Conference, Atlanta, GA, June 23–25, 1997; revision received April 15, 1998; accepted for publication May 4, 1998.

*Research Associate, Alfred Gessow Rotorcraft Center, Glenn L. Martin Institute of Technology; currently Technical Specialist, Aerodynamics and Noise Technology, Boeing Information, Space and Defense Systems, P.O. Box 16858, MS P32-97, Philadelphia, PA 19142-0858. E-mail: Ashish.Bagai@PHL.Boeing.com. Senior Member AIAA.

†Associate Professor, Alfred Gessow Rotorcraft Center, Glenn L. Martin Institute of Technology, Department of Aerospace Engineering. E-mail: leishman@eng.umd.edu. Senior Member AIAA.

limitation of free-wake schemes is the computational expense associated with repetitive induced velocity evaluations. Numerically, the free-vortex filaments are discretized along their lengths into segments connected by collocation points. The total induced velocity field at each collocation point is determined as a sum of the velocity contributions from all of the other vortex elements in the rotor wake. This is done using the Biot–Savart law. Whereas this in itself is not a computationally intensive task on a per element basis, the total number of evaluations required to determine the effects of each vortex element on every collocation point in the wake can incur very large computational costs. Because a typical rotor problem may be modeled using multiple trailed filaments from each blade through several turns of the rotor, the total number of collocation points in the computational domain can easily be in the hundreds of thousands. For aeroacoustic predictions the required minimum azimuthal resolution of the wake may be 1 deg or smaller, and in these cases the number of velocity field evaluations required to compute an entire free-vortex solution for the rotor wake can quickly become prohibitive unless special numerical schemes are developed.

Several attempts have been made to improve computational efficiencies of helicopter rotor free-vortex wake methods. Schemes have been developed to optimize the algorithmic structures and exploit parallel computing capabilities.[34] Other methods have focused on using simplified models based on analytic solutions to ring vortices, allowing limited wake distortion degrees of freedom,[35–37] or by using other analytical approximations for the vortex induced velocities.[17] The most common approach, however, has simply been to reduce the number of induced velocity calculations between vortex filaments and collocation points. This can be done by simply updating the induced velocities less frequently, by using fewer vortex elements and collocation points in the discretized wake, or by subdividing the wake into near-field and far-field regions of weak and strong influence.[38–44] However, although successful in decreasing execution times, the resulting velocity field errors often undermine the accuracy of the final solutions.

This paper discusses the formulation of two new general computational enhancement algorithms that have been developed to accelerate the performance of free-vortex wake models. Although the methods are based on performing fewer Biot–Savart evaluations to reduce execution times, steps have been taken to ensure that neither the generality of the method nor the predictive accuracy of the results are compromised. The schemes have been applied to and evaluated for a pseudoimplicit predictor–corrector (PIPC) free-wake analysis.[45–47] This wake scheme is based on a relaxation approach that has been demonstrated to be numerically robust, very general in application, and physically accurate when compared with experimental measurements. A third method, which exploits the implicitness of the PIPC algorithm, has also been implemented in the present work to further enhance the efficiency of the scheme.

Methodology

To understand the potential gains in computational efficiency that may be realized as a consequence of reducing the number of velocity field evaluations, it is possible to estimate the number of Biot–Savart-like velocity evaluations required for a typical free-wake solution. In a typical discretized free-wake domain, the rotor azimuth and trailed vortex filaments can be divided into a finite number of equal sized angular steps $\Delta\psi$ around the azimuth, and $\Delta\zeta$ along the length of the vortex filament (see Fig. 1). Let $N_\psi = 360\,\text{deg}/\Delta\psi$ be the number of discrete azimuthal grid points. Likewise, for a vortex filament that is n rotor revolutions old, the number of free collocation points (equal to number of free vortex elements on that filament) is $N_\zeta = n360\,\text{deg}/\Delta\zeta$. Therefore, a total of N_ζ^2 Biot–Savart evaluations must be performed for each free-vortex filament at each of N_ψ locations to account for the total self-induced velocities at each collocation point from every other vortex element. Assuming that the wake is modeled using only a single free-vortex filament from each blade tip, this results in $N_\psi N_\zeta^2$ evaluations to define the rotor wake at all azimuth angles. For a rotor with N_b blades, a further $N_b(N_b-1)N_\psi N_\zeta^2$ evaluations must be performed to account for mutually induced effects. Therefore, the total number of Biot–Savart

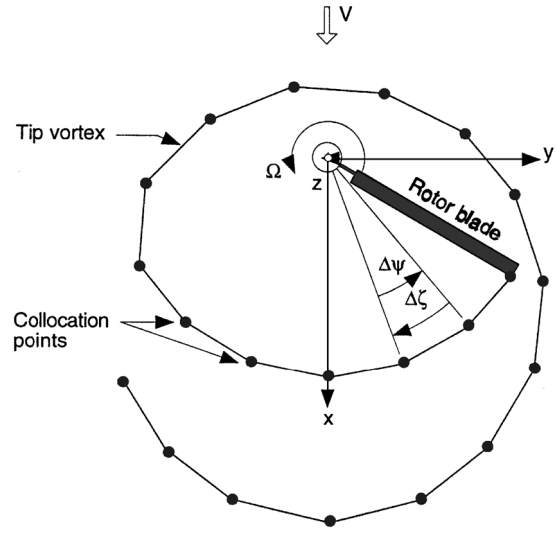

Fig. 1 Rotor azimuth and vortex filament discretization.

evaluations required per free-wake computation, whether using a time-stepping or relaxation approach, is given by the equation

$$N_E = [1 + N_b\,(N_b - 1)]N_\psi N_\zeta^2 \tag{1}$$

For equal step sizes, $\Delta\psi = \Delta\zeta \Rightarrow N_\zeta = nN_\psi$, and so the total number of evaluations becomes

$$N_E = [1 + N_b\,(N_b - 1)]nN_\psi^3 \tag{2}$$

For a typical four-bladed helicopter rotor with three revolutions of free-tip vortices and equal discretization step sizes of 10 deg, Eq. (2) shows that the Biot–Savart integral must be evaluated over 1.8×10^6 times to cover the entire computational domain just once. Doubling the resolution, i.e., using step sizes half the original size, such that $\Delta\psi = \Delta\zeta = 5$ deg, requires eight times that number, or over 14.5×10^6 velocity evaluations. For additional free-vortex filaments, the mutual interactions between all of the additional free vortices must also be computed, leading to very substantial increases in computational effort. Clearly then, even a relatively modest reduction in the number of velocity field evaluations can potentially translate into significant reductions in execution time.

A measure of the gain in computational efficiency can be made in terms of the CPU times required between coarse and refined wake grids. Assuming that the CPU time is directly proportional to the number of operations leads to the hypothesis that the total execution time per wake iteration is directly proportional to the number of mathematical operations that must be performed. The number of operations depends primarily on the number of free collocation points in the wake (rotor azimuthal and vortex filament discretization), which in turn is dependent on the number of vortices trailed from each blade, the trailer lengths, and the discretization step sizes. Based on these proportionality assumptions, and by utilizing Eqs. (1) and (2), a computational cost index (CI) can be defined as a measure of the gain in computational efficiency. Three cost indices can be defined as the reciprocal of the ratios of relative CPU cost, namely,

$$\begin{aligned}
\text{CI}^{-1} &= (\text{CPU}_0/\text{CPU}_1) = \left(N_{E_0}/N_{E_1}\right) = N^3, && \Delta\psi = \Delta\zeta \\
\text{CI}^{-1} &= (\text{CPU}_0/\text{CPU}_1) = \left(N_{E_0}/N_{E_1}\right) = N, && \Delta\psi > \Delta\zeta \\
\text{CI}^{-1} &= (\text{CPU}_0/\text{CPU}_1) = \left(N_{E_0}/N_{E_1}\right) = N^2, && \Delta\zeta > \Delta\psi
\end{aligned} \tag{3}$$

where CPU_0 corresponds to the execution time required for a discretization resolution corresponding to step sizes $\Delta\psi_0$, $\Delta\zeta_0$. CPU_1 is the execution time required for a coarse resolution with step sizes $\Delta\psi_1 = N\Delta\psi_0$ and/or $\Delta\zeta_1 = N\Delta\zeta_0$. From Eq. (3), it is apparent that doubling the azimuthal step size relative to the baseline results in a scheme that requires half the time (on a per iteration basis) of the baseline. Doubling the step sizes in the ζ direction reduces the

CPU time by a factor of four, whereas doubling both the ψ and ζ step sizes increases the computational efficiency eightfold.

The computational enhancement schemes developed in the present work accelerate the free-wake solutions by systematically decreasing the total number of Biot–Savart evaluations, while also maintaining the fidelity of the predictions. Two generic schemes have been developed: 1) an unequal step size discretization scheme using linear velocity field interpolation and 2) an adaptive grid sequencing with iteration scheme. Both of these schemes have been implemented in the PIPC free-wake analysis,[45–47] and the relative improvements in computational efficiency have been quantified relative to a baseline (nonaccelerated) scheme. The third technique, which uses implicit boundary conditions, is specific to the implicitness of the PIPC scheme.

Free-Wake Scheme

The partial differential equation (PDE) governing the convection of the wake filaments can be obtained from the vorticity transport equation. This may be applied to the rotor free-wake problem using a relaxation approach.[45] This results in a hyperbolic PDE of the form

$$\frac{\partial \boldsymbol{r}(\psi,\zeta)}{\partial \psi} + \frac{\partial \boldsymbol{r}(\psi,\zeta)}{\partial \zeta} = (\boldsymbol{V}_\infty + \boldsymbol{V}_{\text{ind}}) \tag{4}$$

The term $\boldsymbol{V}_{\text{ind}}$, on the right-hand side of Eq. (4) is composed of the instantaneous velocity contributions of all of the vortex elements in the wake. The velocity induced at a point located at position $\boldsymbol{r}$ relative to a vortex element $\mathrm{d}\boldsymbol{l}$ is determined using the Biot–Savart law, which can be written as an integral of the form

$$\boldsymbol{V}_{\text{ind}} = \frac{\Gamma}{4\pi}\int \frac{\mathrm{d}\boldsymbol{l}\times\boldsymbol{r}}{|\boldsymbol{r}|^3} \tag{5}$$

where Γ is the strength of the vortex filament. In application, this equation is reduced to one involving a desingularized two-dimensional vortex model[48] and may be rewritten as

$$\boldsymbol{V}_{\text{ind}} = \frac{\Gamma h^2}{4\pi\left(r_c^{2n}+h^{2n}\right)^{1/n}}\int \frac{\mathrm{d}\boldsymbol{l}\times\boldsymbol{r}}{|\boldsymbol{r}|^3} \tag{6}$$

where h is the perpendicular distance of the evaluation point from the influencing vortex element and r_c is the viscous core radius (which is an empirical input). The integer n defines the vortex velocity profile. Note that if $n\to\infty$, the Rankine vortex profile is obtained, and if $n=1$, the Kaufmann or Scully velocity profile is recovered.[39] For the free-wake problem, the induced-velocity term is a function of the relative positions of the vortices in the wake. Equation (4), therefore, is a nonlinear PDE.

The partial derivatives on the left-hand side of Eq. (4) can be discretized in the two spatial directions (ψ and ζ) using a five-point central differencing scheme. This is done by dividing the rotor azimuth into a finite number of blade locations of constant angular step size $\Delta\psi$, and segmenting the trailed vortices in the wake into straight line elements of equal angular increments $\Delta\zeta$. No constraints are placed on the discretization step sizes in the two directions. The resulting spatially discretized finite difference equation (FDE) is given by[45–47]

$$\boldsymbol{r}_{j,k} = \boldsymbol{r}_{j-1,k-1} + (\boldsymbol{r}_{j,k-1} - \boldsymbol{r}_{j-1,k})\left(\frac{\Delta\psi-\Delta\zeta}{\Delta\psi+\Delta\zeta}\right) + \frac{2}{\Omega}\left(\frac{\Delta\psi\Delta\zeta}{\Delta\psi+\Delta\zeta}\right)(\boldsymbol{V}_\infty+\boldsymbol{V}_{\text{ind}}) \tag{7}$$

This FDE now defines the numerical solution to the free-wake problem.

The PIPC algorithm, which is based on a relaxation approach,[45–47] is used to integrate Eq. (7). In this method, the blade azimuth location is fixed in time, and the position of each free collocation point on the corresponding vortex filament is updated. The position vector updates, therefore, proceed along the vortex filament length for each blade azimuth location. The solution then proceeds by relaxation, where the predicted wake geometries are iterated until a converged solution is obtained. Convergence was measured as an L_2-norm or root-mean-square (rms) change in geometries between successive iterations, normalized with respect to the number of free collocation points in the wake and relative to the first iteration rms. A convergence threshold of $L_2 = 10^{-3}$ was specified for all cases, which is low enough to ensure full and proper convergence.

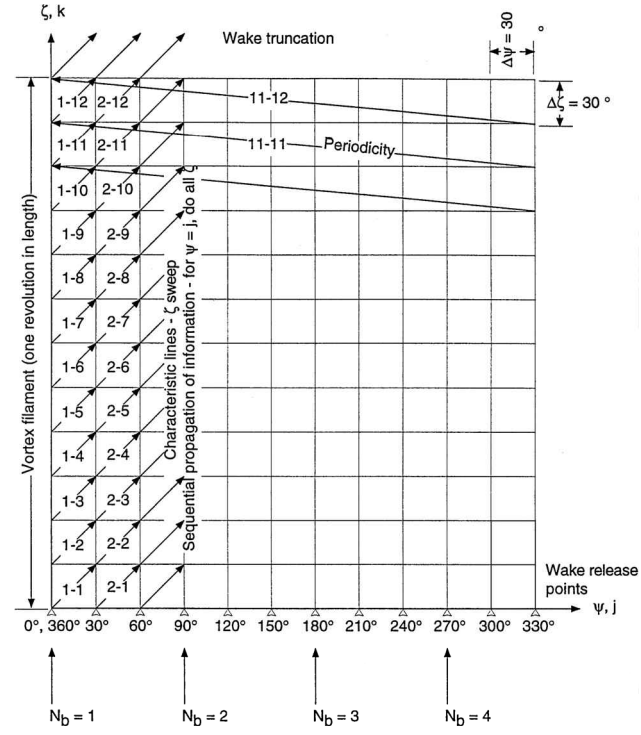

Fig. 2 Propagation of information along characteristic lines in the discretized computational domain.

The general solution concept is shown in Fig. 2, which shows the propagation of information in the computational domain along characteristics in the direction of the vortex filaments, i.e., in the ζ direction. For each $\zeta_{k=1-N_\zeta}$ at a particular ψ_{j+1}, information is used from each corresponding $\zeta_{k=1-N_\zeta}$ at ψ_j and ψ_{j+1}, as dictated by Eq. (7), along with the necessary enforcement of periodicity. Note that the characteristic lines for the free-wake problem can be determined from the general solution of the linearized PDE in Eq. (4) by assuming the right-hand side is constant. It can be shown that these characteristic lines are oriented at an angle of 45 deg (requiring $\Delta\psi = \Delta\zeta$). These characteristics define directions of information propagation along which the hyperbolic PDEs given by Eq. (4) reduce to ordinary differential equations.

Acceleration Schemes

The second term on the right-hand side of Eq. (7) provides an implicit correction factor for the use of unequal step sizes. This corrector function is useful for computing wake solutions at considerable CPU savings. For example, very high azimuthal discretizations might be specified to identify regions of BVIs over the rotor disk, but without incurring the added expense of requiring a fine resolution wake geometry. On the other hand, a high fidelity wake discretization could be used for vortex wake/airframe or rotor/tail rotor interaction studies, but using a lower rotor azimuthal discretization. However, either of these schemes potentially results in a loss of general accuracy because the physical mapping between the length of the vortex element is not preserved relative to the angular distance traveled by the rotor blades. As a consequence, information will be propagated along incorrect characteristic lines.

Linear Velocity Interpolation

The underlying principle for using linear interpolation (LI) with unequal step sizes is to perform fewer explicit induced-velocity evaluations, while retaining the accuracy and fidelity of the wake solution obtained with small equal discretization step sizes. This acceleration scheme uses larger step sizes with LI to map the azimuthal

and vortex filament discretizations and to restore the direction of information propagation to the correct characteristic lines, as for the case for equal step sizes. In such situations, the implicit correction term vanishes, further simplifying the FDEs and recovering the numerical accuracy of equal step size wake solutions.[46] The induced velocity terms, denoted by $\boldsymbol{V}_{\text{ind}}$ in Eq. (7), are treated as before by using velocity averaging and relaxation parameters.[45–47]

Note that the computational economy of an interpolation scheme is a consequence of not having to evaluate the Biot–Savart law for each and every collocation point in the computational domain. The spatial location of every collocation point (whether calculated or interpolated) is still determined using the PIPC relaxation scheme. However, the self- and mutually induced velocity fields are computed only for the free collocation points. LI is used to determine the local induced-velocity field at the interpolated or pseudofree collocation points. This local, interpolated velocity field is then used at the pseudofree collocation points to convect them to force-free locations in the rotor flowfield, just as for the truely free points. Note again, however, that it is not the spatial positions of the collocation points that are being interpolated, but the local velocity field itself.

Azimuthal interpolation, $\Delta\psi > \Delta\zeta$. Interpolation in the azimuthal direction is required when the azimuthal step size is larger than the vortex filament discretization step size, i.e., $\Delta\psi > \Delta\zeta$. The interpolation scheme is applied to both the rotor azimuthal locations and the entire vortex filament. The discretized physical and computational domains are shown in Figs. 3 and 4. The solid symbols represent the explicitly computed collocation points, whereas the open points are those where the induced velocity field is interpolated. It is important to appreciate that the interpolation scheme is applied to determine the local induced-velocity field at each interpolated (open) point and not to directly interpolate the spatial locations. In so doing, all wake collocation points are allowed to convect through the flowfield. Although simple displacement interpolation schemes could have been used, this would have resulted in a wake solution no different than that obtained using a coarse discretization with additional collocation points superimposed on the solution. In such a case, it would not be possible to obtain a solution approaching the predictive accuracy of a high-resolution wake. The gain in computational efficiency for this case, therefore, comes from the savings of performing fewer evaluations of the Biot–Savart integral because it is not evaluated at or between the interpolated points. Note that interpolation is performed between points that lie on different vortex filaments but on the same characteristic line (direction of information propagation), i.e., points C, D, and E are interpolated using information at points A and B.

Special care is required for certain points when interpolating in the azimuthal direction, and these have also been indicated in Figs. 3 and 4. The gray-shaded points are vortex release points, which are determined from the blade locations. This may be done by interpolating the vortex radial release points between calculated blade locations in the azimuthal direction and computing their (exact) locations in space corresponding to the blade azimuthal positions. The local velocities at these points are determined by linearly interpolating the induced velocities between the neighboring release points (solid). Using this release point information, the velocity field at the inner points may then be determined by interpolation.

The last few points on the interpolated vortex filaments (thick-open) cannot be determined conventionally as for the inner points because the computed endpoints are not available from the adjacent computed blade locations. This is a result of wake truncation because each vortex filament is modeled as a finite number of rotor revolutions in length. For these special points, an approximate interpolation is used, as also indicated in Figs. 3 and 4. For example, interpolated velocity information at points c, d, and e are obtained using information from points a and b. Note that this does not introduce any significant errors when computing the rotor airloads for filaments greater than two rotor revolutions in length. Moreover, these interpolated special endpoints are not critical because wake truncation means that the characteristics passing through them do not lead to calculated collocation points.

When applying this interpolation scheme, the characteristic lines of information propagation match the equal step size cases, these concepts are also shown in Figs. 3 and 4 for the case where $\Delta\psi > \Delta\zeta$. Both the discretized physical domain (see Fig. 3) and computational domain (see Fig. 4) serve to demonstrate the underlying principles of the velocity field interpolation scheme.

Vortex filament interpolation, $\Delta\zeta > \Delta\psi$. Interpolation along the vortex filaments is applied when the discretization step in the ζ direction is larger than the discretized azimuthal step size, i.e., $\Delta\zeta > \Delta\psi$. For such cases, collocation points are interpolated between the originally specified, calculated collocation points along the length of the same vortex filaments. For example, points C and D (open) in Figs. 5 and 6 are interpolated using information from

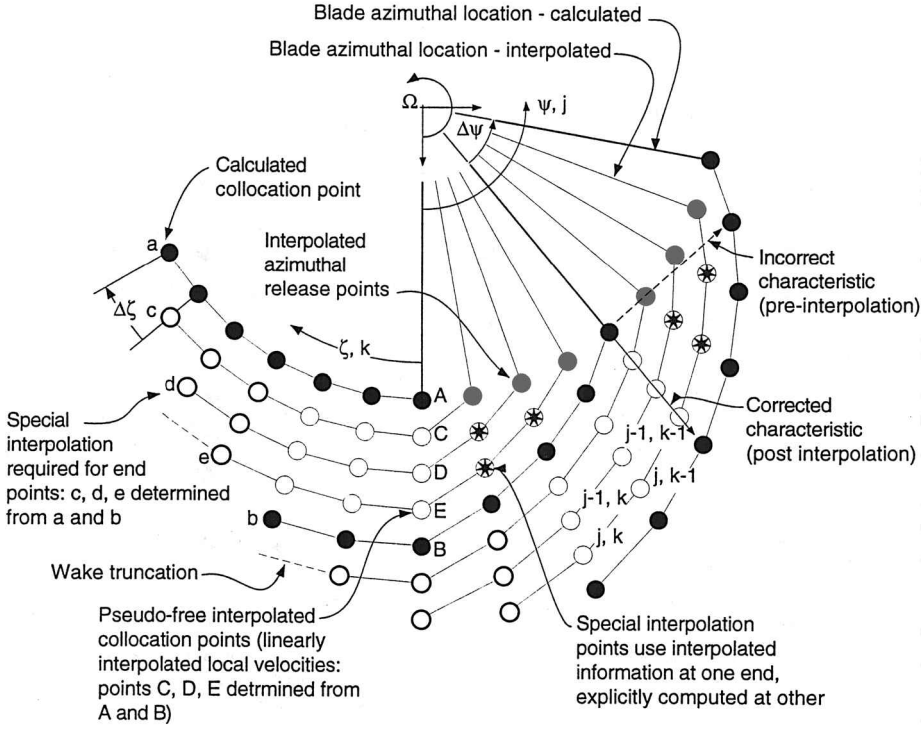

Fig. 3 Discretized physical domain for linear velocity interpolation, $\Delta\psi > \Delta\zeta$.

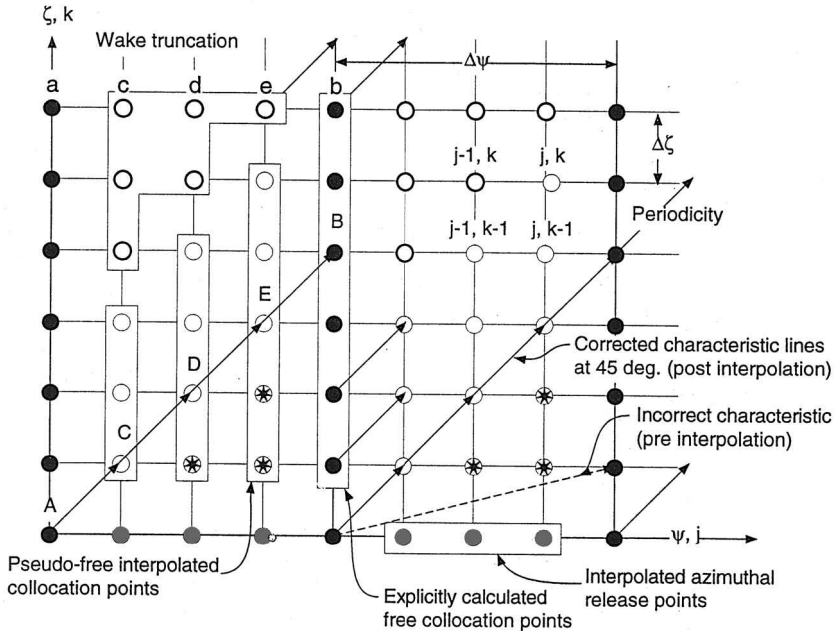

Fig. 4 Discretized computational domain for linear velocity interpolation, $\Delta\psi > \Delta\zeta$.

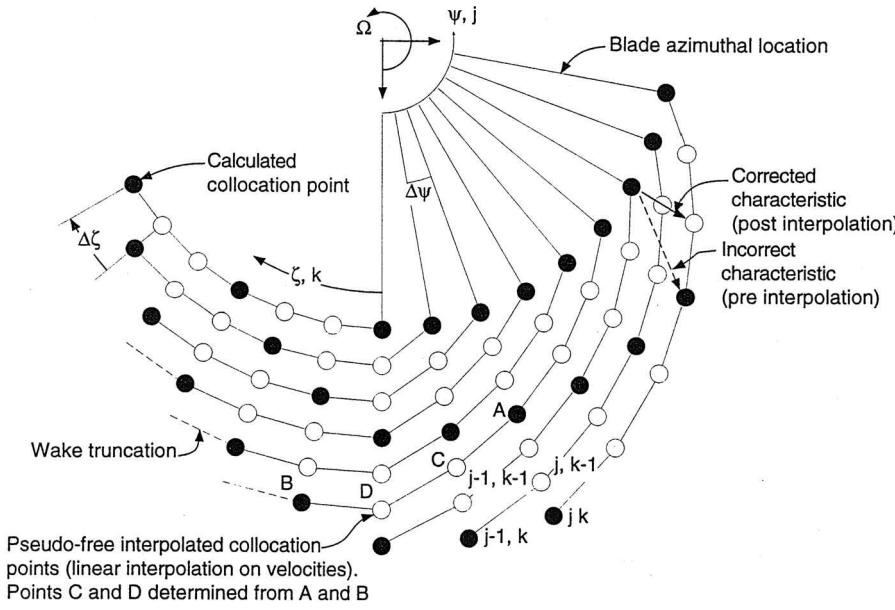

Fig. 5 Discretized physical domain for linear velocity interpolation, $\Delta\psi < \Delta\zeta$.

calculated points A and B (solid) lying on the same vortex filament. The velocity field at each of the calculated, free collocation points is explicitly computed by invoking the Biot–Savart law, and these sparse, free collocation points are, again, assumed to be interconnected by straight line vortex segments. The local induced-velocity field at each of the pseudofree collocation points is linearly interpolated in the ζ direction. This approximate velocity field is then used to convect these points using the pseudoimplicit formulation, as described earlier.

The discretized physical and computational domains are shown in Figs. 5 and 6. The correction to the characteristic lines as a result of interpolation are also indicated. Note, however, that the interpolation scheme for this case is significantly simpler than for the preceding case, where $\Delta\psi > \Delta\zeta$, and no points require special treatment.

Adaptive Grid Sequencing

An adaptive grid sequencing scheme starts the free-wake solution using a coarse grid. As the free-wake iterations proceed, the grid resolution is adaptively refined. Only then are the final few iterations performed at the highest grid resolution. Using a low-resolution grid during the initial iterations provides a better initial condition to begin the subsequent higher resolution iterations. Gains in computational efficiency result as a consequence of faster overall convergence and by performing fewer induced-velocity evaluations.

The initial iterations are performed assuming a relatively coarse level wake. At each iteration, only those rotor azimuthal locations and wake collocation points that correspond to the current level of discretization are treated freely. The predefined interior wake collocation points are not computed explicitly, but are treated as pseudo-free and are allowed to convect through the rotor flow at the interpolated velocity field. When the iteration block corresponding to a given resolution is complete, a new iteration block is then initiated using a higher resolution than before. The solution from the previous iteration is used as a starting value or initial wake geometry for this new iteration block. The process is repeated until the final few iterations are performed at the highest resolution desired. This results in

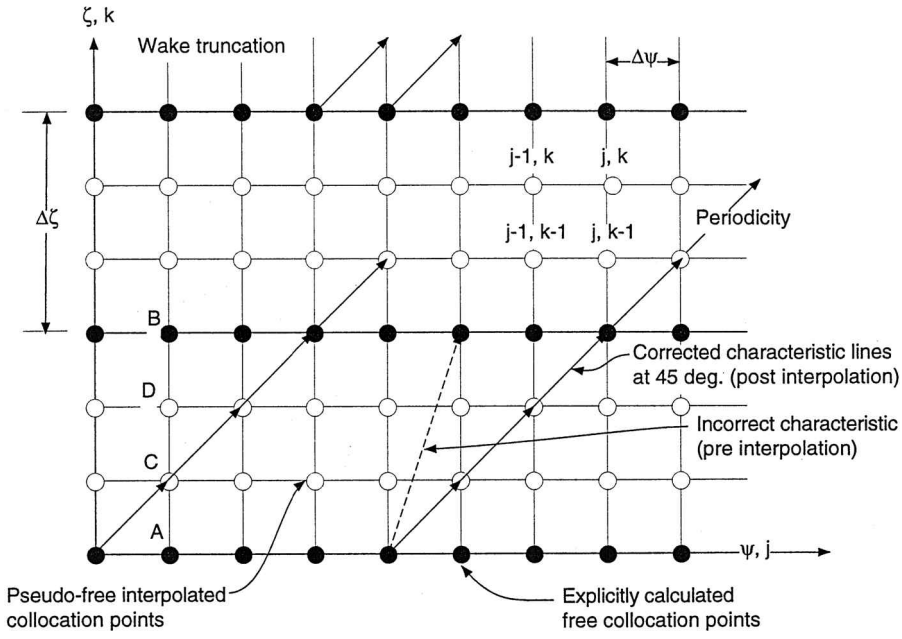

Fig. 6 Discretized computational domain for linear velocity interpolation, $\Delta\psi < \Delta\zeta$.

a wake geometry that is essentially identical to that obtained by performing all of the iterations at the highest resolution. However, the computational expense involved in such a process is significantly less, and up to an order of magnitude reduction is possible.

An alternative to treating the interior points as pseudofree during a coarse resolution iteration would, again, be to simply update their spatial position vectors using linear interpolation between the computed positions. Although such an approach would have the computational economy of not having to apply the free-wake equations to every wake collocation point, the resulting wake solution of each intermediate iteration block would give a substantially inferior initial starting wake for the subsequent higher resolution iterations. Grid sequencing, therefore, also exploits the benefits of velocity field interpolation.

In addition to using equal step sizes in the grid sequencing scheme, unequal step sizes per coarse grid sequencing iteration block can also be used. Again, the approach is similar to that described earlier for the linear interpolation scheme using unequal step sizes, with the final few iterations being performed at the highest grid resolution using equal step sizes.

Implicit Boundary Conditions

The original implementation of the PIPC scheme[45,46] performed collocation point updates by sweeping in the ζ direction, as shown earlier by Fig. 2. However, it is possible to improve the convergence characteristics of the free-wake wake algorithm by rearranging the scheme such that position updates are performed by sweeping in the azimuthal ψ direction, as shown schematically in Fig. 7. By using information at the boundaries that is known previously, the dependency of information from $\zeta_{k=1-N_\zeta}$ at ψ_j can be removed. Instead, the propagation of information along the characteristics is performed at every $\psi_{j=1-N_\psi}$, one ζ_k at a time. Therefore, at every blade azimuthal location, the starting point is now the vortex release point on the blade, which is either specified or known exactly for the current iteration.

Using such an approach introduces an additional degree of implicitness into the solution and is termed implicit boundary conditions (IBC). Wake collocation points are continuously updated in azimuthal sweeps. The use of IBC concepts applicable to the analysis were first suggested by Khanna[49] and Khanna and Baeder[50] to exploit wake symmetry rotations for hover wake predictions. The main advantage of the IBC scheme is the faster propagation of information through the rotor computational domain because it starts from a more accurate (exactly known) boundary condition. Moreover, the dependency on approximate information, as from points $\zeta_{k=1-N_\zeta}$, is eliminated.

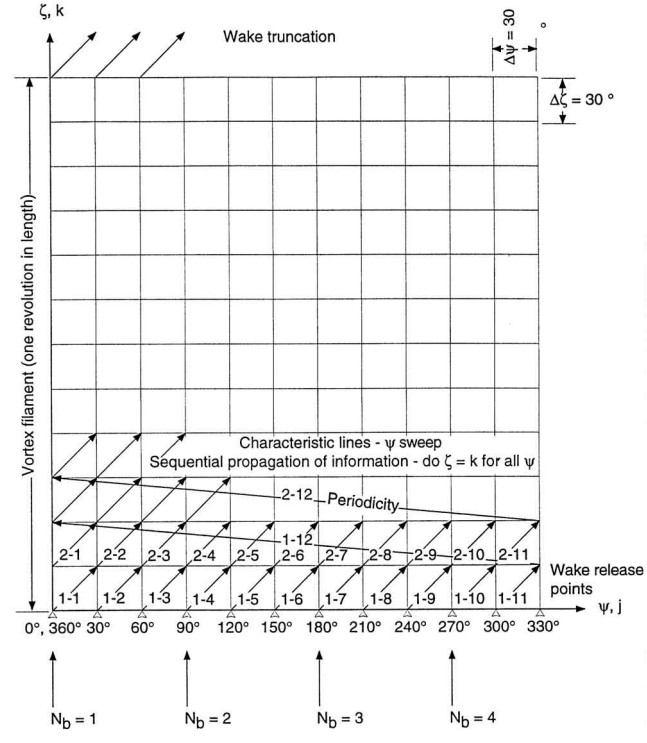

Fig. 7 Propagation of information along characteristic lines in the discretized computational domains using IBCs.

Results and Discussion

The free-wake solutions obtained using the original and IBC schemes were computed for the highest-resolution cases of $\Delta\psi = \Delta\zeta = 2.5$ deg. These solutions are assumed to be exact for the purposes of the present comparisons. In addition to the two baseline schemes, the four accelerated cases evaluated are 1) LI with $\Delta\psi > \Delta\zeta$, 2) LI with $\Delta\psi < \Delta\zeta$, 3) grid sequencing with $\Delta\psi = \Delta\zeta$, and 4) grid sequencing with $\Delta\psi < \Delta\zeta$. All solutions exploit the use of IBCs.

When developing acceleration schemes based on approximate local velocities, some loss in predictive accuracy must be expected. Therefore, steps must be taken to ensure that any loss in accuracy does not result in a nonphysical solution. The IBC and original implementations showed that the predicted wake geometries were

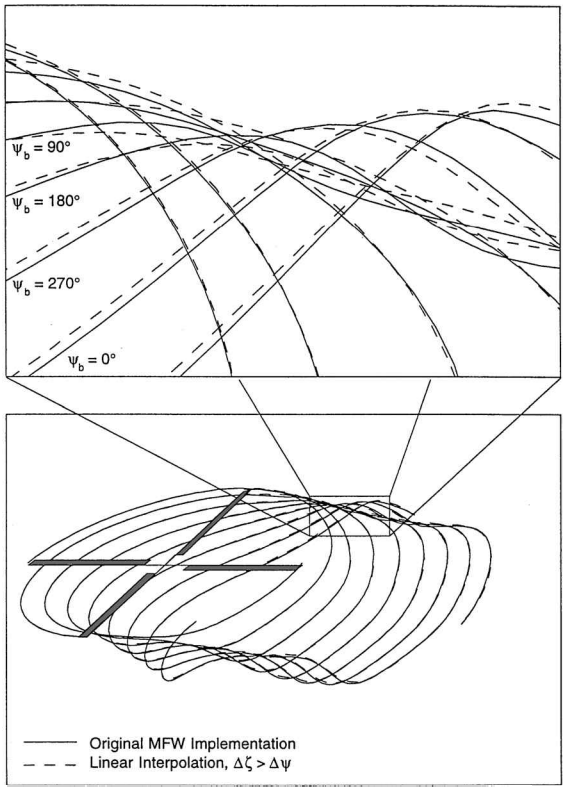

Fig. 8 Predicted wake geometries, original vs LI, $\Delta\zeta > \Delta\psi$; isometric view (bottom) and magnified area (top). Maximum resolution $\Delta\psi = 2.5$ deg $= \Delta\zeta$, two free-wake revolutions, $N_b = 4$, $\mu = 0.1$, $\psi_b = 0$, 90, 180, and 270 deg.

identical. This was to be expected because the only difference between these two schemes was the direction of wake geometry updates, that is, in the ζ direction in the original implementation vs ψ direction for the IBC method.

The wake geometries obtained by using the acceleration schemes, however, differed slightly from those obtained using the baseline implementation. Figure 8 shows typical comparisons between predicted wake geometries obtained using the original scheme and LI with $\Delta\zeta = 4\Delta\psi$. The lower figure shows the wake geometry in isometric form. Although the geometries have been shown for a representative reference blade azimuthal location of $\psi_b = 0$ deg, the geometries are comparable at all azimuthal angles. Also, the final solutions in all cases have been allowed to relax to the same convergence threshold. An enlarged portion of the wake is shown in the upper part of Fig. 8. This area corresponds to a region downstream of the advancing side of the rotor disk, where mutual interactions between the vortex filaments cause the wake to roll up into tight bundles, and the wake undergoes the largest distortions from the epicycloidal form. It can been seen that, even for relatively coarse grids, the interpolated wake geometry compares very well to the exact solution, and for all practical purposes, the differences are negligible.

A contributor to the good agreement found between the accelerated solution and the baseline scheme is the grid-independent behavior exhibited by the original analysis.[51] It has been found that, as the wake resolution is increased (step sizes made smaller), the predicted wake geometries approach a single solution. For example, consider three equal grid resolutions of $\Delta\psi = \Delta\zeta = 10$, 5, and 2.5 deg (the exact physical result is approached as the step sizes become infinitesimal, provided no singularities exist). The wake geometries using the three discretizations are plotted in Fig. 9. Again, the upper part of Fig. 9 is a greatly magnified view of part of the wake structure. Only a single tip vortex trailed from a blade azimuthal location at $\psi_b = 0$ deg is shown for clarity. It is apparent from Fig. 9 that the solutions obtained using the three step sizes are nearly identical, with any differences diminishing rapidly as the wake resolution is increased. The collocation points corresponding to the 5-deg resolution lie almost exactly on top of the wake structure corresponding

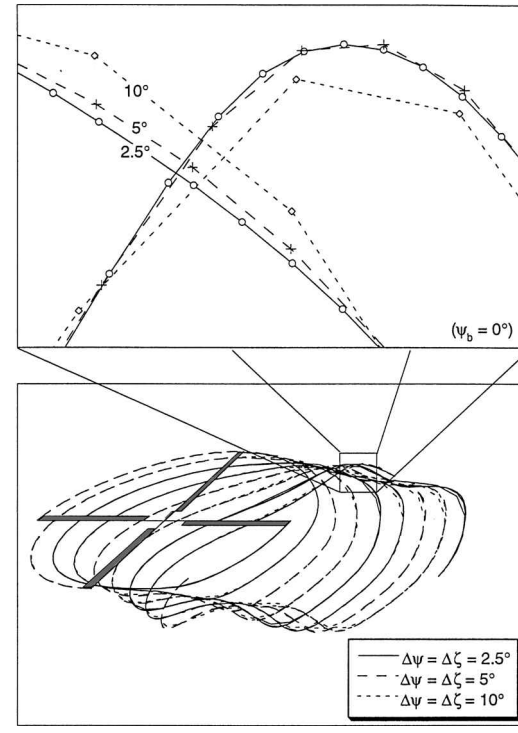

Fig. 9 Grid independency; isometric view (bottom) and magnified view of tip vortices from $\psi_b = 0$ deg (top).

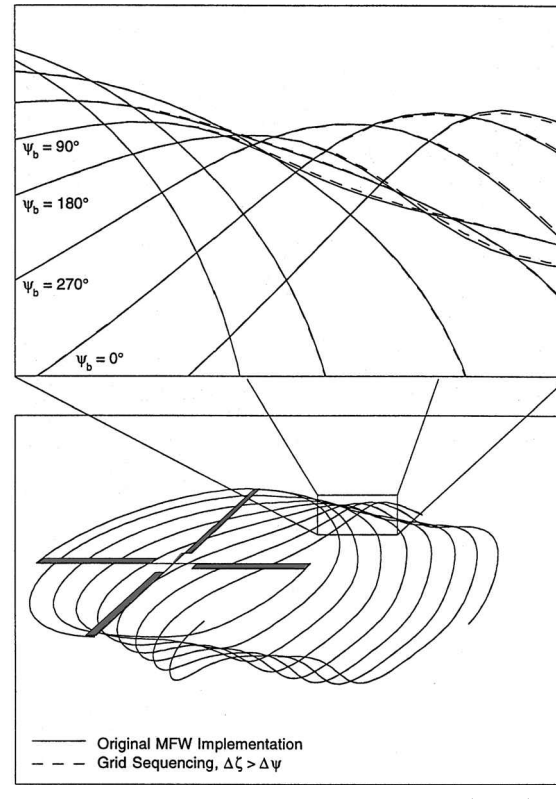

Fig. 10 Predicted wake geometries, original vs GS, $\Delta\zeta > \Delta\psi$; isometric view (bottom) and magnified area (top). Maximum resolution $\Delta\psi = 2.5$ deg $= \Delta\zeta$, two free-wake revolutions, $N_b = 4$, $\mu = 0.1$, $\psi_b = 0$, 90, 180, and 270 deg.

to the 2.5-deg resolution. Some differences, although noticeable in Fig. 9, are actually very small and are primarily a result of the self-induced velocity errors incurred by neglecting the contributions of vortex elements immediately adjacent to a collocation point.

Figure 10 shows similar comparisons between the original implementation and grid sequencing (GS) with $\Delta\zeta > \Delta\psi$. Here the differences are even smaller than for the LI scheme. This, however, is to be expected because the final few iterations using GS

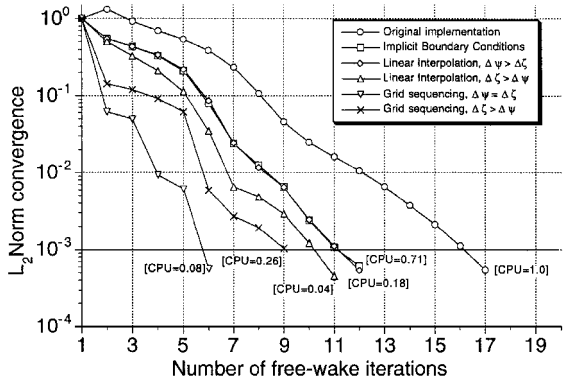

Fig. 11 Free-wake convergence trends.

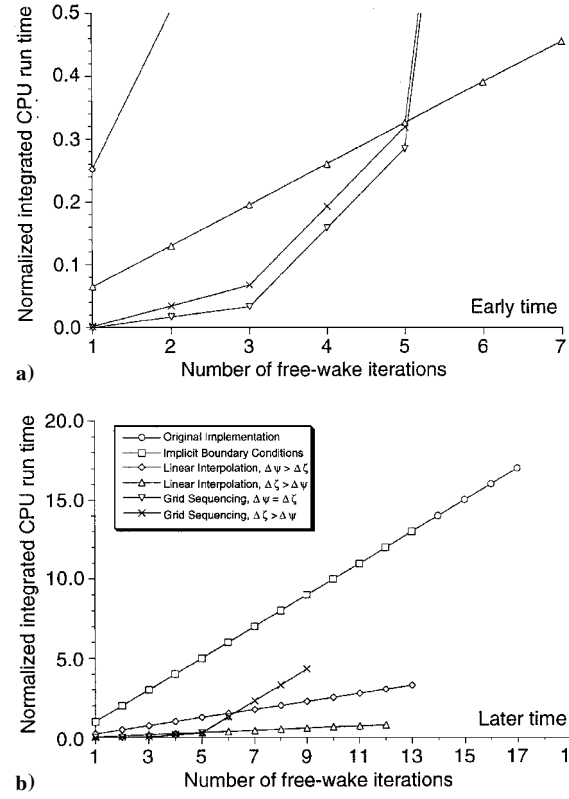

Fig. 12 Cumulative normalized CPU time comparisons through convergence.

are performed at the highest resolution discretization. In general, predicted wake geometries using the acceleration schemes demonstrated no significant loss in accuracy compared to the baseline free-wake implementation.

One of the most striking differences between the original and IBC solutions are the different rates of convergence to arrive at the same result. Because both schemes were run for the same high-resolution discretizations, the CPU time reductions in the IBC case result entirely from the fewer number of wake iterations required for convergence. As shown in Fig. 11, the accelerated free-wake schemes show different convergence trends that warrant additional explanation. These manifest as changes in convergence rates and differences in CPU time requirements. As is apparent for the accelerated schemes, faster convergence rates do not necessarily translate into greater computational efficiency (a reduction in net CPU time). For example, GS using equal step sizes has the highest rate of convergence (requiring only 6 iterations to converge to the final geometry), but LI with $\Delta\zeta > \Delta\psi$ takes 11 iterations. However, the latter scheme converges almost twice as fast as the GS method, as indicated by the CPU time in Fig. 11.

These relative CPU differences between the methods described are a direct consequence of the different number of induced-velocity evaluations performed, which is directly proportional to the number of free collocation points in the wake. Insight into the increase in computational efficiency that results from the acceleration schemes can be gained by plotting the integrated CPU time with iteration number, as shown in Fig. 12. The data presented here are the cumulative CPU time requirements as the free-wake iterations proceed, and the data are normalized by the CPU time required for one iteration of the baseline (or IBC) unaccelerated wake solutions. Figure 12a helps delineate the trends between the integrated CPU curves for the initial iterations; Fig. 12b shows results for later iterations.

Figure 12 shows that the different acceleration schemes manifest as different CPU time requirements on a per iteration basis. The linear interpolation scheme with $\Delta\zeta > \Delta\psi$ runs at a constant per iteration cost through convergence, and so Fig. 12 shows a linear increase in CPU time with iteration. On the other hand, the GS scheme with equal step sizes shows a piecewise linear integrated CPU curve. During the initial coarse resolution blocks, the unit CPU requirements of the GS method are negligible. As the sequencing scheme proceeds and the discretization resolution is increased, the per iteration unit cost cumulatively increases, adding to the total CPU time. Ultimately, the last GS iteration, which is performed at the highest desired resolution, has the highest CPU overheads and crosses over the LI scheme curve. Because the final iteration point of the integrated CPU curves is indicative of the total costs incurred in obtaining a solution, it is evident that the GS scheme takes longer in absolute time than the LI scheme. However, it converges to the same solution in considerably fewer iterations.

Whereas there are substantial differences in the total CPU costs associated with the two GS schemes as well, this results primarily from the three extra high-resolution iterations that the second GS scheme requires to converge to the same tolerance (see Fig. 12a). Because these high-resolution iterations are the most expensive, the total CPU requirements of the latter sequencing scheme are substantially higher. On a per iteration basis, however, Fig. 12b shows that the two schemes are comparable in computational cost.

Summary and Conclusions

Three numerical schemes have been formulated to accelerate and improve the computational efficiency of helicopter rotor free-wake analyses. These were an unequal discretization step-size scheme using LI, an adaptive GS scheme, and an implicit boundary condition approach. The reasons for developing such methods are to accelerate convergence trends and to reduce the number of computationally expensive operations that must be performed to obtain a converged rotor wake solution. The schemes have permitted high-fidelity wake predictions with little or no loss in accuracy and at considerably lower CPU run times relative to the original (nonaccelerated) wake analysis.

The following conclusions have been drawn from this work:

1) The CPU time required to obtain a free-wake solution is directly proportional to the number of velocity field operations that must be performed. A reduction in the rotor azimuthal resolution results in a proportional increase in computational efficiency. The same reduction in vortex filament resolution results in a squared increase in efficiency, whereas combined azimuthal and vortex filament effects result in a cubed efficiency gain.

2) Velocity field interpolation schemes result in reduced costs per iteration by performing fewer explicit induced-velocity calculations. However, every collocation point is allowed to convect through the computational domain using either explicitly calculated induced velocities or approximated (linearly interpolated) velocities. Using velocity field interpolation with $\Delta\psi = N\Delta\zeta$ results in an Nth-order reduction in CPU time, whereas using interpolation with $\Delta\zeta = N\Delta\psi$ results in a N^2 reduction in run time. This is not a consequence of the slightly different interpolations required for the two methods.

3) GS proved to greatly enhance the computational efficiency of the free-vortex wake analysis. The primary reduction in execution times results during the initial wake relaxation process, which uses coarse levels of discretization. As the wake relaxes, the resolution is increased by progressively introducing additional free-wake collocation points into the solution. Only the final few iterations through

convergence are run at the highest desired resolution. GS was found to require considerably fewer wake iterations to converge to a unique solution compared with the other schemes.

4) The IBC method resulted in accelerated convergence, requiring fewer wake iterations to obtain the same unique solution as the original (nonaccelerated) free-wake implementation. The use of IBCs changes the direction of information propagation from along the vortex filament lengths to the azimuthal direction, thereby exploiting the use of exact information from the specified boundary conditions.

5) From the results presented, it is the authors' opinion that the accuracy of the final free-wake solutions were sufficiently refined for all cases. Therefore, the scheme of choice becomes the one offering the greatest reduction in CPU run time. This has been shown to be the LI method using unequal step sizes with $\Delta\zeta > \Delta\psi$. Clearly, as the results presented reflect, the tradeoff in using an acceleration scheme can be some degradation in the quality of the final solution as compared with the unaccelerated baseline/original case.

Acknowledgments

This work was supported by the Aeroacoustics Branch, Fluid Mechanics and Acoustics Division, NASA Langley Research Center, under Contract 01-5-26360. Thomas F. Brooks was the Technical Monitor. The authors would like to thank James Baeder for helpful discussions on the numerical aspects of the problem and Harsh Khanna for his insight into the use of implicit boundary conditions.

References

[1]Leishman, J. G., and Bagai, A., "Challenges in Understanding the Vortex Dynamics of Helicopter Rotor Wakes," *AIAA Journal*, Vol. 36, No. 7, 1998, pp. 1130–1140 (AIAA Paper 96-1957).

[2]Schmitz, F. H., *Aeroacoustics of Flight Vehicles, Theory and Practice, Vol. 1, Noise Sources*, NASA Reference Publication 1258, 1991, pp. 65–149.

[3]Ward, J. F., "Helicopter Rotor Periodic Differential Pressures and Structural Response Measured in Transient and Steady-State Maneuvers," 26th Annual National Forum of the American Helicopter Society, June 1970.

[4]Curtiss, H. C., Jr., and Quackenbush, T. R., "The Influence of the Rotor Wake on Rotorcraft Stability and Control," 15th European Rotorcraft Forum, Paper 70, Amsterdam, The Netherlands, Sept. 1989.

[5]Spencer, R. H., "Application of Vortex Visualization Techniques to Rotor Noise Research," 25th Annual National Forum of the American Helicopter Society, May 1969.

[6]Egolf, T. A., and Sparks, S. P., "A Full Potential Rotor Analysis with Wake Influence Using an Inner–Outer Domain Technique," 42nd Annual National Forum of the American Helicopter Society, Washington, DC, June 1986.

[7]Wake, B. E., and Sankar, L. N., "Solutions of the Navier–Stokes Equations for the Flow About a Rotor Blade," *Journal of the American Helicopter Society*, Vol. 34, No. 2, 1989, pp. 13–23.

[8]Srinivasan, G. R., and Baeder, J. D., "Recent Advances in Euler and Navier–Stokes Methods for Calculating Helicopter Rotor Aerodynamics and Acoustics," 4th International Symposium on Computational Fluid Dynamics, Davis, CA, Sept. 1991.

[9]Duque, E. P. N., and Srinivasan, G. R., "Numerical Simulation of a Hovering Rotor Using Embedded Grids," 48th Annual National Forum of the American Helicopter Society, Washington, DC, June 1992.

[10]Ahmad, J., and Duque, E. P. N., "Helicopter Rotor Blade Computation in Unsteady Flows Using Moving Embedded Grids," AIAA Paper 94-1928, June 1994.

[11]Srinivasan, G. R., Baeder, J. D., Obayashi, S., and McCroskey, W. J., "Flowfield of a Lifting Rotor in Hover: A Navier–Stokes Simulation," *AIAA Journal*, Vol. 30, No. 10, 1992, pp. 2371–2378.

[12]Strawn, R. C., and Barth, T. J., "A Finite-Volume Euler Solver for Computing Rotary-Wing Aerodynamics on Unstructured Meshes," *Journal of the American Helicopter Society*, Vol. 38, No. 2, 1993, pp. 61–67.

[13]Wake, B. E., and Baeder, J. D., "Evaluation of a Navier–Stokes Analysis Method for Hover Performance Prediction," *Journal of the American Helicopter Society*, Vol. 31, No. 1, 1996, pp. 7–17.

[14]Landgrebe, A. J., "An Analytical and Experimental Investigation of Helicopter Rotor Performance and Wake Geometry Characteristics," Eustis Directorate, U.S. Army Air Mobility Research and Development Lab., USAAMRDL TR 71-24, June 1971.

[15]Kocurek, J. D., and Berkowitz, L. F., "Velocity Coupling—A New Concept for Hover and Axial Flow Wake Analysis and Design," CP-334, AGARD, May 1982.

[16]Egolf, T. A., and Landgrebe, A. J., "Helicopter Rotor Wake Geometry and Its Influence in Forward Flight, Vol. I—Generalized Wake Geometry and Wake Effect on Rotor Airloads and Performance," NASA CR-3726, Oct. 1983.

[17]Beddoes, T. S., "A Wake Model for High Resolution Airloads," International Conf. on Rotorcraft Basic Research, Triangle Park, NC, Feb. 1985.

[18]Batchelor, G. K., *An Introduction to Fluid Dynamics*, Cambridge Univ. Press, Cambridge, England, UK, 1967, p. 264.

[19]Scully, M. P., "A Method of Computing Helicopter Vortex Wake Distortion," Massachusetts Inst. of Technology, Rept. ASRL TR 138-1, Cambridge, MA, June 1967.

[20]Bliss, D. B., Quackenbush, T. R., and Bilanin, A. J., "A New Methodology for Helicopter Free Wake Analysis," 39th Annual National Forum of the American Helicopter Society, St. Louis, MO, May 1983.

[21]Bliss, D. B., Wachspress, D. A., and Quackenbush, T. R., "A New Approach to the Free Wake Problem for Hovering Rotors," 41st Annual National Forum of the American Helicopter Society, Ft. Worth, TX, May 1985.

[22]Bliss, D. B., Dadone, L., and Wachspress, D. A., "Rotor Wake Modeling for High Speed Applications," 43rd Annual National Forum of the American Helicopter Society, St. Louis, MO, May 1987.

[23]Johnson, W. R., "Wake Model for Helicopter Rotors in High Speed Flight," NASA CR-177507, USAVSCOM TR-88-A-008, Nov. 1988.

[24]Quackenbush, T. R., Bliss, D. B., Wachspress, D. A., and Ong, C. C., "Free Wake Analysis of Hover Performance Using a New Influence Coefficient Method," NASA CR-4309, July 1990.

[25]Miller, W. O., and Bliss, D. B., "Direct Periodic Solutions of Rotor Free Wake Calculations," *Journal of the American Helicopter Society*, Vol. 38, No. 2, 1993, pp. 53–60.

[26]Crouse, G. L., Jr., and Leishman, J. G., "A New Method for Improved Free-Wake Convergence in Hover and Low Speed Forward Flight," AIAA 31st Aerospace Sciences Meeting and Exhibit, Reno, NV, Jan. 1993.

[27]Quackenbush, T. R., Lam, C. M. G., Wachspress, D. A., and Bliss, D. B., "Analysis of High Resolution Unsteady Airloads for Helicopter Rotor Blades," 50th Annual National Forum of the American Helicopter Society, Washington, DC, May 1994.

[28]Clark, D. R., and Leiper, A. C., "The Free Wake Analysis—A Method for the Prediction of Helicopter Rotor Hovering Performance," *Journal of the American Helicopter Society*, Vol. 15, No. 1, 1970, pp. 3–11.

[29]Sadler, S. G., "A Method for Predicting Helicopter Wake Geometry, Wake-Induced Flow and Wake Effects on Blade Airloads," 27th Annual Forum of the American Helicopter Society, Washington, DC, May 1971.

[30]Sadler, S. G., "Development and Application of a Method for Predicting Rotor Free Wake Positions and Resulting Rotor Blade Air Loads," Model and Results, Vol. 1, NASA CR-1911, Dec. 1971.

[31]Sadler, S. G., "Main Rotor Free Wake Geometry Effects on Blade Air Loads and Response for Helicopters in Steady Maneuvers," Theoretical Formulation and Analysis of Results, Vol. 1, NASA CR-2110, Sept. 1972.

[32]Berry, J. D., "Prediction of Time-Dependent Fuselage Pressures in the Wake of a Helicopter Rotor," 2nd International Conf. on Rotorcraft Basic Research, Univ. of Maryland, College Park, MD, Feb. 1988.

[33]Egolf, T. A., "Helicopter Free Wake Prediction of Complex Wake Structures Under Blade–Vortex Interaction Operating Conditions," 44th Annual Forum of the American Helicopter Society, Washington, DC, June 1988.

[34]Egolf, T. A., and Massar, J. P., "Helicopter Free Wake Implementation on Advanced Computer Architecture," 2nd International Conf. on Rotorcraft Basic Research, Univ. of Maryland, College Park, MD, Feb. 1988.

[35]Miller, R. H., "A Simplified Approach to the Free Wake Analysis of a Hovering Rotor," *Vertica*, Vol. 6, 1982, pp. 89–95.

[36]Miller, R. H., "Vortex Theory for Hovering Rotors," *AIAA Journal*, Vol. 20, No. 12, 1982, pp. 1754–1756.

[37]Miller, R. H., "Application of Fast Free Wake Analysis Techniques to Rotors," *Vertica*, Vol. 8, No. 3, 1984, pp. 255–261.

[38]Landgrebe, A. J., "An Analytical Method for Predicting Rotor Wake Geometry," *Journal of the American Helicopter Society*, Vol. 14, No. 4, 1969, pp. 20–32.

[39]Scully, M. P., "Computation of Helicopter Rotor Wake Geometry and Its Influence on Rotor Harmonic Airloads," Massachusetts Inst. of Technology, ASRL TR 178-1, Cambridge, MA, March 1975.

[40]Johnson, W., "A Comprehensive Analytical Model of Rotorcraft Aerodynamics and Dynamics, Part I: Analysis Development," NASA TM-81182, June 1980.

[41]Bliss, D. B., Teske, M. E., and Quackenbush, T. R., "A New Methodology for Free Wake Analysis Using Curved Vortex Elements," NASA CR-3958, Dec. 1987.

[42]Chua, K., and Quackenbush, T. R., "A Fast Three-Dimensional Vortex Method for Unsteady Wake Calculations," AIAA Paper 92-2624, June 1992.

[43]Bliss, D. B., and Miller, W. O., "Efficient Free Wake Calculations Using Analytical/Numerical Matching," *Journal of the American Helicopter Society*, Vol. 38, No. 2, 1993, pp. 43–52.

[44]Miller, W. O., "A Fast Adaptive Resolution Method for Efficient Free Wake Calculations," 49th Annual National Forum of the American Helicopter Society, St. Louis, MO, May 1993.

[45]Bagai, A., and Leishman, J. G., "Rotor Free-Wake Modeling Using a Pseudo-Implicit Technique—Including Comparisons with Experiment," *Journal of the American Helicopter Society*, Vol. 40, No. 3, 1995, pp. 29–41.

[46]Bagai, A., and Leishman, J. G., "Rotor Free-Wake Modeling Using a Pseudo-Implicit Relaxation Algorithm," *Journal of Aircraft*, Vol. 32, No. 6, 1995, pp. 1276–1285.

[47]Bagai, A., and Leishman, J. G., "Free-Wake Analysis of Tandem, Tilt-Rotor and Coaxial Rotor Configurations," *Journal of the American Helicopter Society*, Vol. 41, No. 3, 1996, pp. 196–207.

[48]Vatistas, G. H., Kozel, V., and Mih, W. C., "A Simpler Model for Concentrated Vortices," *Experiments in Fluids*, Vol. 11, 1991, pp. 73–76.

[49]Khanna, H., "Coupled Wake/CFD Solutions for Rotors in Hover," M.S. Thesis, Dept. of Aerospace Engineering, Univ. of Maryland, College Park, MD, 1996.

[50]Khanna, H., and Baeder, J. D., "Coupled Free-Wake/CFD Solutions for Rotors in Hover Using a Field Velocity Approach," 52nd Annual Forum of the American Helicopter Society, June 1996.

[51]Bagai, A., "Contributions to the Mathematical Modeling of Rotor Flow-Fields Using a Pseudo-Implicit Free-Wake Analysis," Ph.D. Dissertation, Dept. of Aerospace Engineering, Univ. of Maryland, College Park, MD, 1995.

J. Kallinderis
Associate Editor